Anisotropic polarizability of Dy at 532 nm on the intercombination transition

Damien Bloch,[1,*] Britton Hofer,[1] Sam R. Cohen,[2,†] Maxence Lepers,[2] Antoine Browaeys,[1] and Igor Ferrier-Barbut[1,‡]
[1]*Université Paris-Saclay, Institut d'Optique Graduate School, CNRS, Laboratoire Charles Fabry, 91127 Palaiseau, France*
[2]*Laboratoire Interdisciplinaire Carnot de Bourgogne, CNRS, Université de Bourgogne, 21078 Dijon, France*

(Received 16 April 2024; accepted 24 July 2024; published 5 September 2024)

We report experimental measurements of the dynamical polarizability of dysprosium, at a wavelength of 532 nm. We measure all three components (scalar, vector, and tensor) of the anisotropic polarizability for the ground and the excited manifolds of the intercombination transition of Dy at 626 nm. The apparatus on which the measurements are performed is presented. We obtain with this setup imaging of single Dy atoms with fidelity above 99% and losses below 2.5% induced by imaging. We then describe the methods used to extract the polarizability. In particular, we combine a measurement of trap frequency and trap depth on single atoms in optical tweezers, allowing us to obtain a measurement of the ground-state polarizability free of errors in trap waist calibration. The obtained values give a magic condition between two Zeeman states in the ground and excited manifolds, which is used to image single atoms in optical tweezer arrays. The scalar polarizability of the ground state is in disagreement with theoretical expectations, calling for future investigations to resolve the discrepancy.

DOI: 10.1103/PhysRevA.110.033103

I. INTRODUCTION

In recent years, cold-atom experiments using lanthanide atoms have made possible the exploration of a wide variety of problems in quantum physics due to their large spin and high magnetic moment [1]. New experimental setups are now required for the application of state-of-the-art atomic physics tools such as optical tweezer arrays [2–4] or quantum gas microscopy [5,6] to lanthanides. The latest was recently adapted [7,8], and we reported the trapping of single dysprosium atoms in optical tweezer arrays in [9].

Here we present the apparatus on which single Dy atoms in optical tweezer arrays are produced. It is based on a three-dimensional magneto-optical trap (MOT) inside a glass cell loaded by a two-dimensional (2D) MOT, similar to the methods reported in Ref. [10]. Narrow-line imaging in optical tweezers is strongly impacted by the trap light shift and hence requires knowledge of the atomic polarizability. We measure the anisotropic polarizability at a trapping wavelength of 532 nm for the ground and excited manifolds of the intercombination line of Dy at 626 nm. From the measured values we identify a magic light polarization for which the lowest Zeeman states of each manifold have the same polarizability, which allows for single-atom imaging in the optical tweezers. We finally compare the experimental values to the theoretical predictions, finding disagreement in the ground state in particular. This highlights the need for future research to understand the value of the polarizability of Dy at 532 nm.

II. EXPERIMENTAL SETUP

For the first laser cooling stages of the experiment, we use the broad blue transition of ^{162}Dy between the manifolds $G = 4f^{10}6s^2\,{}^5I_8$ and $F = 4f^{10}(^5I_8)6s6p(^1P_1^o)\ (8,1)_9^o$ [see Fig. 1(a)]. Its wavelength is $\lambda = 421$ nm and its linewidth is $\Gamma_{421} = 2\pi \times 32$ mHz. We also make use of the narrower intercombination line at $\lambda = 626$ nm between G and $E = 4f^{10}(^5I_8)6s6p(^3P_1^o)\ (8,1)_9^o$ with linewidth $\Gamma_{626} = 2\pi \times 135$ kHz. This transition is used to realize a 3D MOT and to image the atoms in the optical tweezers. The optical tweezers themselves are realized with far-detuned light at 532 nm.

A. Apparatus overview

To trap and image single atoms, the combination of a glass cell and a microscope objective has emerged as a versatile solution offering high optical access and compactness [3,11–13]. Such a platform is desirable for lanthanide atoms to perform single-atom trapping and imaging in tweezers. One experimental challenge faced in adapting these setups to lanthanides such as Er or Dy is that any surface in line of sight of the oven will be coated by the high atomic flux due to their very high melting point. This prevents placing a glass surface or glass cell in front of the atomic jet of the oven. In order to directly load a glass cell, the solution we implement here is a 2D MOT of Dy similar to the one reported in Ref. [10], which serves as a continuous source of cold Dy atoms pushed towards the glass cell.[1] This alleviates the need for optical transport and so ensures high experiment repetition rates (greater than 1 Hz). The vacuum system (LEOS)

*Contact author: damien.bloch@institutoptique.fr
†Present address: Department of Physics, Stanford University, Stanford, California 94305, USA.
‡Contact author: igor.ferrier-barbut@institutoptique.fr

[1]It is also possible to place a 45° mirror inside the glass cell [8], but this imposes stringent requirements on the glass cell making.

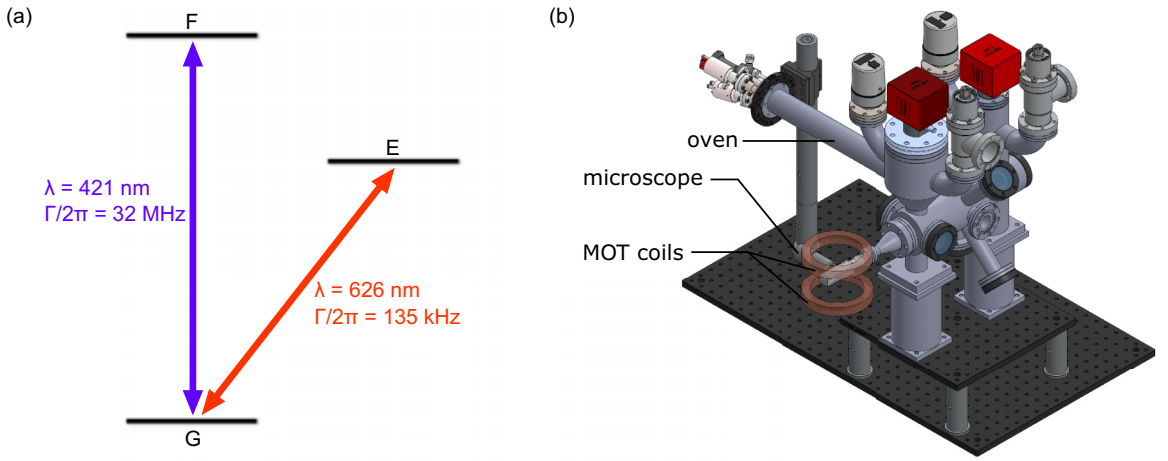

FIG. 1. (a) Optical transitions of Dy used in this work. (b) Sketch of the vacuum system.

was adapted from a similar design for Strontium [14,15]. It consists of two parts separated by a differential pumping section [see Fig. 1(b)]. The first section is a stainless-steel chamber in which a high-temperature oven loads a 2D MOT of Dy. The oven (Createc DFC-40-25-WK-2) is made of an effusion cell containing the solid Dy and a hotter lip near the front of the oven to prevent Dy deposit from clogging the output. The effusion cell is loaded with 70 g of Dy and heated up to 900 °C during normal operation, while the hot lip is held at 1200 °C. The chamber is designed such that the output of the oven is only 7 cm away from the center of the 2D MOT, in order to mitigate the effect of the flux divergence at the output of the oven. The 2D MOT chamber is made of a main cylinder with eight radially pointing flanges welded to provide a connection for the oven and access for the 2D MOT beams, as well as additional optical access to image the 2D MOT. A near-resonant beam on the 421-nm transition is also sent through a viewport to push the atoms from the 2D MOT through the differential pumping section and towards the glass cell in which they are trapped in a 3D MOT. The science cell (ColdQuanta $10 \times 13 \times 60$ mm^3) is surrounded by a pair of anti-Helmholtz coils that produces the quadrupole magnetic gradient for the 3D MOT. In addition, three pairs of Helmholtz coils are used to control the homogeneous offset field in the cell. The 3D MOT is used to load atoms in optical tweezers, which are made by focusing light at 532 nm through a microscope objective (Mitutoyo G Plan APO 50×) with a 0.5 numerical aperture (NA), which we also use to capture single-atom fluorescence [9]. We review below the main stages of the experiment.

B. The 2D MOT

The velocity of the atoms coming out of the oven is about 400 m s^{-1}. To capture the largest fraction of these atoms, we use a 2D MOT on the broad 421-nm transition. The cooling light is made of a single beam passing in a bow-tie configuration [10]. The Gaussian beam waist is 8 mm and its power is 300 mW ($I = 5I_{\text{sat}}$). It is detuned by $\Delta = -3.2\Gamma_{421}$ from the transition. The magnetic field of the 2D MOT is generated with four stacks of five permanent magnets placed on the corners of a rectangle with a width of 7 cm and a height of 9 cm in the XZ plane. These magnets generate a theoretical magnetic gradient of 23 G/cm in the Y and Z directions. With these parameters, the capture velocity of the 2D MOT is on the order of 100 m s^{-1}. This is visible in Fig. 2, which shows simulated trajectories of atoms coming out of the oven and crossing the 2D MOT region. The simulations are performed using the PYLCP package [16].

To load the 3D MOT in the glass cell, the atoms are pushed in the nonconfining direction of the 2D MOT by a near-resonant beam on the 421-nm transition. The glass cell is 30 cm away from the 2D MOT, and the 3D MOT beam radius is about 5 mm. To prevent atoms from dropping under gravity below the 3D MOT beams, they must be accelerated to a velocity $v \gtrsim 15$ m s^{-1}. The push beam has a waist of $w_{\text{push}} = 1.2$ mm, a detuning of $\Delta_{\text{push}} = -1.9\Gamma_{421}$, and an intensity of 0.7 mW ($I_{\text{push}} = 0.55I_{\text{sat}}$). With these parameters, the velocity reached by the atoms is close to 20 m s^{-1}. To prevent the radiation pressure of this push beam from disturbing the 3D MOT in the glass cell, we angle it by about 5 ° so that it does not pass through the differential pumping section and thus does not reach the cell [17].

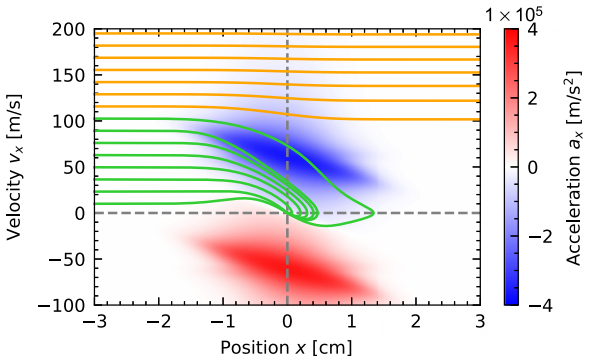

FIG. 2. Simulated phase-space trajectories in the 2D MOT in the plane $(x, z) = 0$. Green lines are trajectories of atoms with incoming velocity below the capture velocity of the 2D MOT. Orange lines are trajectories of atoms that are too fast to be captured by the 2D MOT and just fly through it. The red and blue colormap indicates the acceleration experienced by the atoms due to the 2D MOT light.

C. Core-shell MOT

In the glass cell, we realize a 3D MOT on the 626-nm transition whose relatively narrow linewidth of 135 kHz results in a low Doppler temperature $T_D \simeq 3.2$ μK [18,19]. However, this linewidth comes also at the cost of a low capture velocity. The waist of the MOT beams is limited to about $w \simeq 1$ cm by the size of the cell. This yields a capture velocity $v_c \sim \sqrt{\hbar k \Gamma w/m} \lesssim 10\ \mathrm{m\,s^{-1}}$, lower than the minimum velocity for the atoms to reach the cell. Modulating the MOT frequency [18,19] or using very high light intensity [10] cannot bridge this gap. To circumvent this limitation and efficiently capture atoms in the 3D MOT, we realize a core-shell MOT [20] on the 421- and 626-nm transitions. It consists of a hollow outer shell of 421-nm light with a core of 626-nm light. Atoms coming from the 2D MOT are efficiently slowed down by the 421-nm shell and can then accumulate in the 626-nm core. The advantage of this configuration is that we benefit from the high capture velocity afforded by the large scattering rate of the blue transition while avoiding losses due to light-induced collisions and pumping to metastable states [21,22].

To realize this core-shell MOT, we overlap on the horizontal 626-nm MOT beams two retroreflected beams at 421 nm with waists of $w_{421} = 1.5$ cm and whose centers are blocked by masks with a diameter of 5 mm. A blue beam on the vertical direction is not necessary since the vertical velocity of the atoms is low. We find an optimal magnetic gradient for this bicolor MOT to be $B'_{CS} = 5\ \mathrm{G\,cm^{-1}}$. The detuning for the 626-nm MOT during the loading stage is $\Delta_{626} = -40\Gamma_{626}$ and the intensity of each beam is $I_{626} = 100 I_{sat,626}$. The detuning of the 421-nm shell is $\Delta_{421} = -1.3\Gamma_{421}$, with a power of about 5 mW per beam (including the blocked central part). We observe about a 100-fold increase in atom number when the core of this MOT is not exposed to 421-nm light, demonstrating the reduction of losses by blocking the central part of the blue beams. Once the 3D MOT is loaded, we abruptly turn off the 2D MOT beams, the push beam, and the 3D MOT capture shell to stop the loading. We then slowly ramp the parameters of the 626-nm MOT over 80 ms to a gradient of $1.7\ \mathrm{G\,cm^{-1}}$, a detuning of $-7.4\Gamma_{626}$, and a light intensity of $I = 3I_{sat,626}$. After this step, the atoms are polarized in the lowest Zeeman state $|G, J = 8, m_J = -8\rangle$ [18,19].

D. Optical tweezers

In the next step of the experiment we load single Dy atoms in optical tweezers. The loading procedure is detailed in [9]. Briefly, the tweezer array is generated at 532 nm, using an acousto-optic deflector (AOD) to generate a 1D or 2D array of tweezers, focused by a 0.5-NA microscope objective. The tweezers are loaded from the MOT as described in [9]. They are imaged with a single nonretroreflected beam at 626 nm with an intensity $I = 0.5 I_{sat,626}$ and a detuning $\Delta = -1.0\Gamma_{626}$. Figure 3(a) shows a histogram of the collected photons for a given trap over many realizations of the experiment, with the typical bimodal distribution illustrating the random loading of each tweezer. Having improved the imaging setup with respect to [9], we now obtain a 2.5% loss probability, after taking a 30-ms-long image, and an imaging fidelity above 99%. As shown in [9], the losses are mainly due to two-photons events during which an atom in the excited state of the 626-nm transition can absorb a trap photon at 532 nm and decay to highly excited metastable states. Since these states have a lifetime of several seconds, the atom will not be detected in the following pictures and is registered as a loss. The same mechanism was observed for Yb [13].

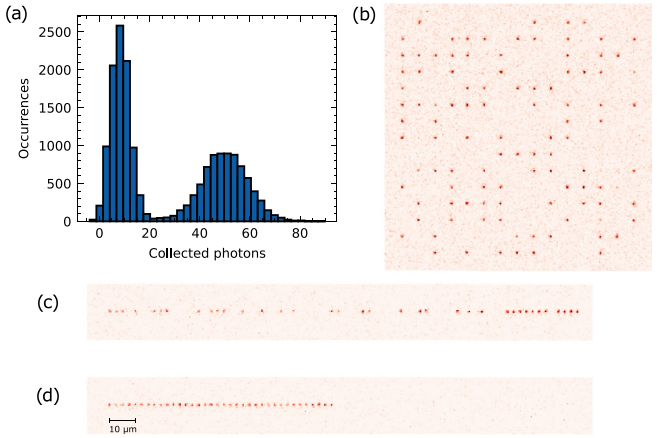

FIG. 3. (a) Histogram of the collected fluorescence for a given trap over many realizations of the experiment. (b) Single shot picture of a 15 × 15 array of traps randomly loaded. Also shown is a single shot picture of an array of 75 traps (c) before and (d) after sorting the traps.

Representative images of a randomly loaded 2D and 1D array are shown in Figs. 3(b) and 3(c). Figure 3(d) shows a typical example of a picture obtained after rearranging the tweezers in one dimension using the technique presented in [3].

A crucial ingredient for the loading and imaging of single atoms using a cooling transition with a linewidth on the order of 100 kHz is to obtain a magic trapping condition [13,23]. The differential light shift between the ground and excited states can be of the order of several megahertz in optical tweezers with a depth of a few hundred microkelvins. This is large compared to the linewidth $\Gamma_{626} = 2\pi \times 135$ kHz of the intercombination transition at 626 nm. Therefore, this differential shift significantly alters the effect of resonant light on the atoms. It was found for the intercombination line of Yb with a similar linewidth (182 kHz) that the magic condition (zero differential light shift) is necessary for single-atom imaging [13,24], and we experimentally found the same to be true for Dy. Finding this magic ellipticity requires the knowledge of the scalar, tensor, and vector polarizabilities of the ground- and excited-state manifolds of the intercombination line. We explain in the next section the experimental measurements which allowed us to extract these six polarizabilities at 532 nm. From these values we have found a magic ellipticity of the tweezer light for which the ground state $|g\rangle = |G, J = 8, m_J = -8\rangle$ and the excited state $|e\rangle = |E, J = 9, m_J = -9\rangle$ have equal total polarizability.

III. POLARIZABILITIES AT 532 nm

Lanthanides are known to feature a highly anisotropic light-matter interaction [25]. For atom trapping with dipole traps, this anisotropy manifests in a strong dependence on

light polarization via the vector and tensor components as was observed, for instance, for Er or Dy [26–30]. Optical traps for Dy are often in the near infrared at 1070 or 1064 nm [31]. For a trap light at $\lambda_{\text{trap}} = 532$ nm, it is known that the ground state of Dy has a positive polarizability so that atoms can be trapped [32,33]. However, the exact value of the polarizability was not precisely measured at this wavelength for either the ground state or the excited state of the intercombination transition.

The effect of the anisotropic polarizability is well described by a light-shift Hamiltonian $\hat{H}_{ls}$ that acts separately on each (hyper)fine structure manifold $\hat{H}_{ls} = \hat{H}_S + \hat{H}_V + \hat{H}_T$ that depends on the scalar vector and tensor polarizabilities α_S, α_V, and α_T as [34,35]

$$\begin{aligned}\hat{H}_S &= -\alpha_S \frac{I}{2c\varepsilon_0},\\ \hat{H}_V &= -i\alpha_V \frac{I}{2c\varepsilon_0}(\boldsymbol{\epsilon}^* \times \boldsymbol{\epsilon}) \cdot \frac{\hat{\boldsymbol{J}}}{2J},\\ \hat{H}_T &= -\alpha_T \frac{I}{2c\varepsilon_0} \frac{3\{\boldsymbol{\epsilon} \cdot \hat{\boldsymbol{J}}, \boldsymbol{\epsilon}^* \cdot \hat{\boldsymbol{J}}\} - 2\hat{\boldsymbol{J}}^2}{2J(2J-1)},\end{aligned} \tag{1}$$

where I is the light intensity, $\boldsymbol{\epsilon}$ is the complex polarization of the electric field, $\hat{\boldsymbol{J}}$ is the atomic spin, and $\{\hat{A}, \hat{B}\} = \hat{A}\hat{B} + \hat{B}\hat{A}$ is the anticommutator between two operators $\hat{A}$ and $\hat{B}$. In the presence of a magnetic field, as is the case for our experiments, the total Hamiltonian can be expressed as

$$\hat{H}_{\text{tot}} = \hat{H}_0 + \hat{H}_{ls},$$

where $\hat{H}_0 = \hbar g_J \mu_B \hat{\boldsymbol{J}} \cdot \boldsymbol{B}$ is the Zeeman Hamiltonian.

In general, the light-shift Hamiltonian does not commute with the Zeeman Hamiltonian. We work here in a regime where the Zeeman shift (approximately $\mu_B B g_J m_J > 40$ MHz for $|m_J| = 8$ $B > 3$ G) is much larger than the vector or tensor light shift (approximately $\alpha_V \frac{I}{2c\varepsilon_0} m_J/J$ or approximately $\alpha_T \frac{I}{2c\varepsilon_0} m_J^2/J^2$, a few megahertz at most) such that the eigenstates of the total Hamiltonian are always close to the Zeeman states.[2] In these conditions, the effect of the light-shift Hamiltonian can be described simply as a first-order energy shift of the Zeeman states and the trapping potential created by a dipole trap follows $V(\boldsymbol{r}) = -\alpha \frac{I(\boldsymbol{r})}{2c\varepsilon_0}$ with a polarizability α that depends on the tweezer polarization and the Zeeman state m_J. In particular, we find that atoms in the most negative Zeeman state $m_J = -J$ experience an effective polarizability

$$\alpha = \alpha_S - i\frac{\alpha_V}{2}(\boldsymbol{\epsilon}^* \times \boldsymbol{\epsilon}) \cdot \boldsymbol{b} + \frac{\alpha_T}{2}[3(\boldsymbol{\epsilon} \cdot \boldsymbol{b})(\boldsymbol{\epsilon}^* \cdot \boldsymbol{b}) - 1], \tag{2}$$

where $\boldsymbol{b} = \boldsymbol{B}/\|\boldsymbol{B}\|$ is the direction of the magnetic field.

Since the direction of the magnetic field plays an important role in our measurement, we carefully calibrate the applied magnetic fields using Zeeman spectroscopy in order to compensate for stray fields. Below we report measurements of the scalar, vector, and tensor polarizabilities for both the ground state G and the upper state E of the intercombination line in a trap with a wavelength of 532 nm for ^{162}Dy. To do so, we first perform experiments in a dipole trap containing many atoms. The atoms are imaged in time of flight so that the magic condition is not required and we can vary the trap polarization. We increase the size of the trap by reducing the input pupil of the microscope with an iris, from an initial NA of 0.5 to an effective NA of about 0.2. In this case, the trap intensity can be modeled by an Airy pattern for which the radial and axial intensity profiles near the center of the trap are given by

$$I(r, z=0) = I_0 \left(\frac{2J_1(kr\eta)}{kr\eta}\right)^2 \tag{3}$$

and

$$I(r=0, z) = I_0 \text{sinc}^2\left(\frac{kz\eta^2}{4}\right), \tag{4}$$

respectively, where η is the numerical aperture, $k = 2\pi/\lambda_{\text{trap}}$ is the wave vector for the trapping light, $I_0 = Pk^2\eta^2/4\pi$ is the peak intensity, P is the trap power, and J_1 is the Bessel function of the first kind with order 1. We find that this intensity profile matches better what is observed in the experiment than what a Gaussian profile predicts. In a test setup reproducing the experimental conditions, we measure the intensity profile and verify that it matches an Airy profile.

A. Measurement of polarizabilities of the ground state G

To estimate the ground-state polarizabilities, we measure the mechanical oscillation frequencies of the dipole trap for atoms in the state $|g\rangle = |G, J=8, m_J=-8\rangle$ at different trap polarizations. The frequencies of the trap are obtained by approximating the potential experienced by the atom with a harmonic potential $V(\boldsymbol{r}) \simeq -U_0 + \frac{1}{2}m\omega_\perp^2(x^2+y^2) + \frac{1}{2}m\omega_\parallel^2 z^2$. In this equation, m is the atomic mass, $\omega_\perp = k\eta\sqrt{\frac{U_0}{2m}}$ and $\omega_\parallel = k\eta^2\sqrt{\frac{U_0}{24m}}$ are the radial and axial trap frequencies, respectively, and $U_0 = \frac{\alpha I_0}{2c\varepsilon_0}$ is the trap depth.

To measure the trap frequencies, we use parametric heating by modulating the trap intensity by 10% of its nominal value for 50 ms, at variable frequencies. A typical measurement of the remaining atom number after modulation as a function of modulation frequency is shown in Fig. 4, showing dips at twice the axial [Fig. 4(a)] and radial [Fig. 4(b)] frequencies of the trap.

The power in the tweezer for the measurements presented in this part is $P = 14(3_{\text{sys}})$ mW. The uncertainty in experimental values is written in parentheses following the measured value. In this case, it is a systematic uncertainty coming from the estimated transmission of the beam path. In addition, the fact that the atoms are not trapped precisely at the trap bottom, combined with the fact that the trap is not perfectly harmonic, creates a systematic error in the obtained frequency [31]; we estimate a 10% systematic error in our experiments.

The ratio of frequencies yields the effective numerical aperture of the trap $\eta = 2\sqrt{3}\omega_\parallel/\omega_\perp = 0.182(20_{\text{sys}})(6_{\text{stat}})$ in agreement with our expectation. Here the two values in parentheses refer to the systematic and statistical uncertainties, respectively. To analyze the data below, we use this experimental value to infer the trap intensity using Eqs. (3) and (4).

To extract the polarizabilities of the ground state, we first perform experiments with a linear trap polarization $\boldsymbol{\epsilon}$. In this

[2]We also performed full diagonalization of the Hamiltonian *a posteriori* to verify that this assumption is correct.

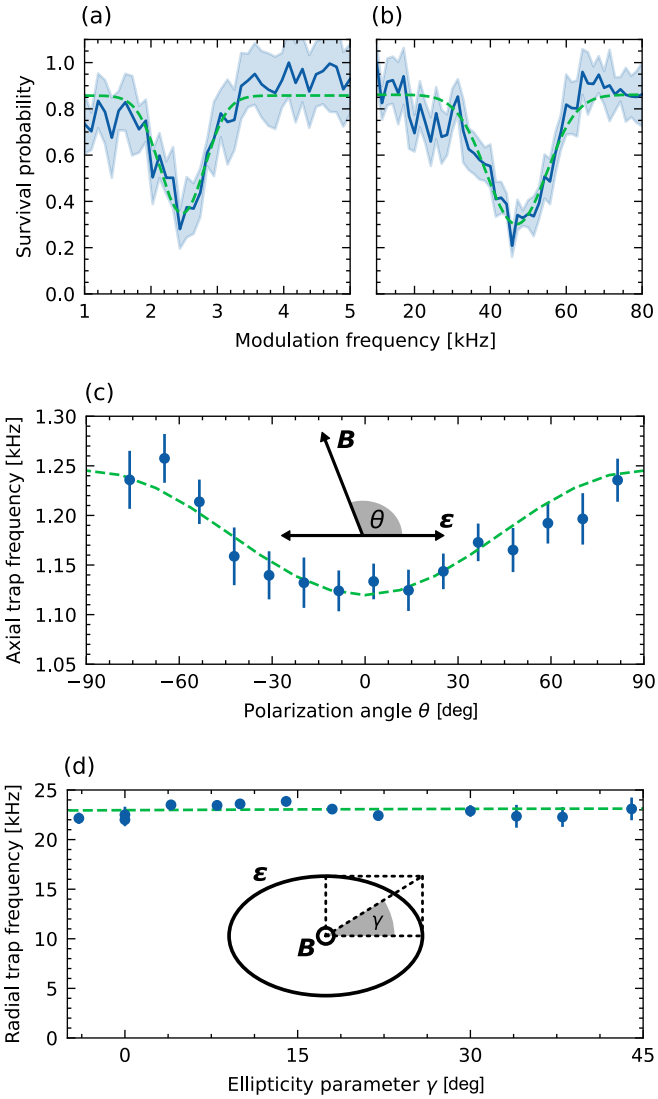

FIG. 4. Measurement of the (a) axial and (b) radial oscillation frequencies in the ground state using parametric heating for a tweezers power $P = 14$ mW. The dashed lines are fits to Gaussian dips in order to locate the resonant modulation frequency. We measure significant losses when we modulate the trap intensity at $2.47(7_{\mathrm{sys}})(2_{\mathrm{stat}})$ and $47(5_{\mathrm{sys}})(1_{\mathrm{stat}})$ kHz, corresponding to twice the axial frequency and twice the radial frequency, respectively. (c) Axial trap frequency for atoms in the state $|G, J, m_J = -J\rangle$ as a function of the angle θ between the trap linear polarization $\boldsymbol{\epsilon}$ and the quantization axis defined by the magnetic field $\boldsymbol{B}$. Blue dots are experimental points. The green dashed line is a fit to Eq. (6). (d) Radial trap frequency in the state $|G, J, m_J = -J\rangle$ as a function of the ellipticity parameter γ. Blue dots are experimental points. The green dashed line is a fit to Eq. (8) and appears flat due to the negligible vector polarizability in the ground state.

case, the vector contribution to the light shift vanishes and the potential experienced by an atom in $m_J = -8$ is

$$V^{\mathrm{lin}}(\boldsymbol{r}) = -\frac{I(\boldsymbol{r})}{2c\varepsilon_0}\left(\alpha_S^G + \frac{\alpha_T^G}{2}[3\cos^2(\theta) - 1]\right), \tag{5}$$

where θ is the angle between the polarization of the trapping light and the magnetic field $\boldsymbol{B}$. We change the value of the parameter θ by rotating the magnetic field with respect to a fixed tweezer polarization. For each angle we measure the axial trap frequency [see Fig. 4(c)] and we fit the obtained data to

$$\omega_{\parallel}(\theta) = \omega_{\parallel,0}\sqrt{1 + \frac{\alpha_T^G}{2\alpha_S^G}[3\cos^2(\theta) - 1]}. \tag{6}$$

From this analysis we find $\omega_{\parallel,0} = 2\pi \times 1.21(10_{\mathrm{sys}})(2_{\mathrm{stat}})$ kHz. This yields $\alpha_S^G = 150(100_{\mathrm{sys}})(30_{\mathrm{stat}})\alpha_0$, with $\alpha_0 = 1.649 \times 10^{-41}\ \mathrm{C^2\,m^2\,J^{-1}}$ the atomic unit of polarizability. Similarly, the fitted curve gives us $\alpha_T^G/\alpha_S^G = -0.14(6_{\mathrm{stat}})$. It is worth noting that there is a large systematic error for the absolute polarizabilities due to the uncertainty in the light intensity at the position of the atoms, but this unknown does not affect the ratio of the two polarizabilities.

To measure the vector polarizability α_V^G, the trap polarization must have a circular component. We use an elliptical polarization in the plane perpendicular to the magnetic field $\boldsymbol{B} = B\boldsymbol{e}_z$ aligned to the tweezer axis:

$$\boldsymbol{\epsilon} = \cos(\gamma)\boldsymbol{e}_x + i\sin(\gamma)\boldsymbol{e}_y.$$

By scanning the parameter γ from 0° to 45°, the polarization can be changed from linear to circular. The potential experienced by atoms in the $|G, J, m_J = -J\rangle$ state is

$$V^{\mathrm{el}}(\boldsymbol{r}) = -\frac{I(\boldsymbol{r})}{2c\varepsilon_0}\left(\alpha_S^G - \frac{\alpha_T^G}{2} + \frac{\alpha_V^G}{2}\sin(2\gamma)\right). \tag{7}$$

We modify this ellipticity parameter by sending the tweezer beam through a quarter waveplate with variable angle. We repeat the measurement of the trap frequencies for different ellipticity parameters γ by rotating the quarter waveplate and fit the resulting radial trap frequencies [Fig. 4(d)] to

$$\omega_{\perp}(\gamma) = \omega_{\perp,0}\sqrt{1 + \frac{\alpha_V^G}{2\alpha_S^G - \alpha_T^G}\sin(2\gamma)}. \tag{8}$$

As visible in Fig. 4(d), the dependence of the trap frequency on γ is smaller than experimental uncertainties, yielding a very small vector polarizability in the ground state: $\frac{\alpha_V^G}{2\alpha_S^G - \alpha_T^G} = 0.01(4_{\mathrm{stat}})$.

B. Differential polarizabilities on the intercombination transition

Once the polarizabilities of the ground state G have been measured, we use these values to deduce the polarizabilities of the excited state E. To do this, we measure the differential light shift on the $|g\rangle = |G, J = 8, m_J = -8\rangle \leftrightarrow |e\rangle = |E, J' = 9, m_J' = -9\rangle$ transition in the trap. When shining 626-nm light on many atoms in the trap, losses are induced if the light frequency is resonant with a transition between the ground state and the excited state. Figure 5 shows an example of such an experiment. In this case, we apply a magnetic field of 3 G to separate the σ_+, σ_-, and π transitions. We then shine 626-nm light at $I \simeq 5I_{\mathrm{sat},626}$ for 20 ms and observe atomic losses when the frequency of this light is resonant with a transition between Zeeman levels of the ground states and excited

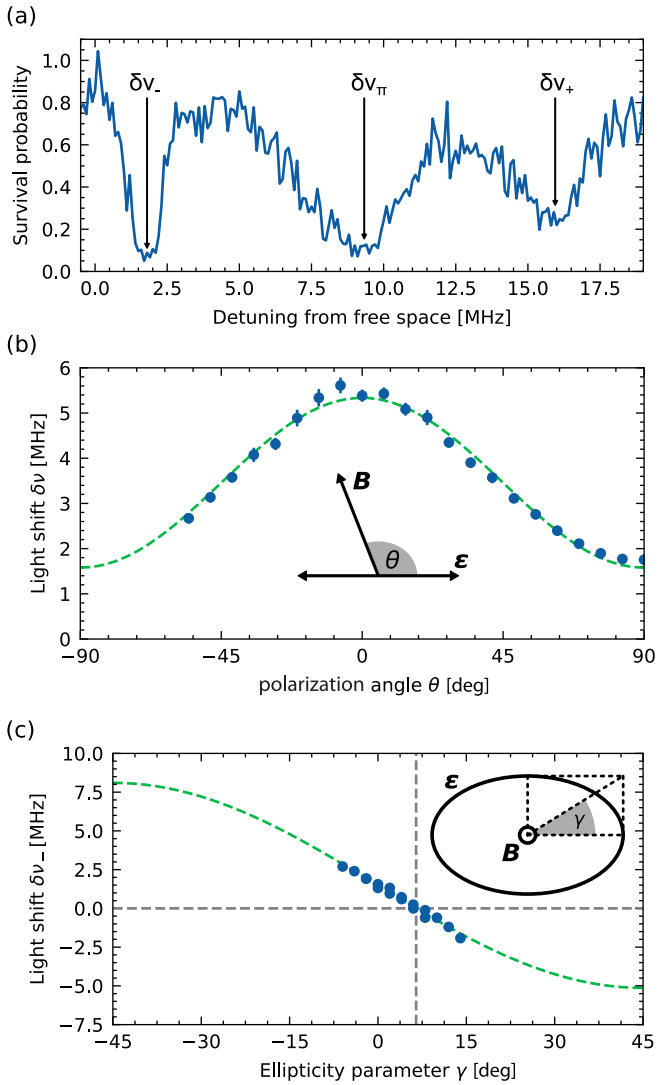

FIG. 5. (a) Induced losses in the dipole trap when shining 626-nm light as a function of light frequency. The effective numerical aperture used here is 0.18 and the tweezer power is $P = 33$ mW. (b) Differential light shift between $|G, J, m_J = -J\rangle$ and $|E, J', m'_J = -J'\rangle$ for a linear polarization as a function of θ. (c) Differential light shift between $|g\rangle$ and $|e\rangle$ for an elliptical polarization as a function of γ. Blue dots are experimental points. The green dashed line is a fit to Eq. (10).

states. The effective $\eta = 0.18$ used for these measurements is the same as above and the power of the dipole trap beam is $P = 33(6_{\text{sys}})$ mW. The frequency is referenced from the frequency of the transition $|g\rangle \leftrightarrow |e\rangle$ in free space. There are three dips in the signal, corresponding to the three projections of the 626-nm light polarization onto the magnetic field axis. Since the atoms are pumped in the $|g\rangle$ state in the MOT before being loaded in the trap, only the σ_- transition is cycling. Atoms interacting with σ_+ and π light are pumped towards other m_J states, causing a broadening of these two transitions. We therefore rely only on the frequency of the σ^- transition to extract the differential polarizability.

We measured the differential light shift again for different polarizations of the trap beam. In Fig. 5(b) we rotate the magnetic-field direction with respect to a linear trap polarization to measure the differential scalar and tensor polarizabilities $\Delta\alpha_S = \alpha_S^{\text{E}} - \alpha_S^{\text{G}}$ and $\Delta\alpha_T = \alpha_T^{\text{E}} - \alpha_T^{\text{G}}$, respectively. We fit this curve to

$$\delta\nu(\theta) = \frac{V_E^{\text{lin}}(0) - V_G^{\text{lin}}(0)}{h} = \delta\nu_0\left(1 + \frac{\Delta\alpha_T}{2\Delta\alpha_S}[3\cos^2(\theta) - 1]\right) \tag{9}$$

and find $\delta\nu_0 = -\Delta\alpha_S I_0/2hc\varepsilon_0 = 2.83(3_{\text{stat}})$ MHz and $\frac{\Delta\alpha_T}{\Delta\alpha_S} = 0.86(3_{\text{stat}})$. Assuming that the intensity is given by Eqs. (3) and (4), this gives $\Delta\alpha_S = -50(14_{\text{sys}})(3_{\text{stat}})\alpha_0$.

To measure the differential vector polarizabilities $\Delta\alpha_V = \alpha_V^{\text{E}} - \alpha_V^{\text{G}}$, we perform a similar measurement, now changing the ellipticity parameter of the trap polarization. This is again done in a configuration where the polarization ellipse is perpendicular to the magnetic field [see Fig. 5(c)]. These values are fitted to

$$\delta\nu(\gamma) = \frac{V_E^{\text{el}}(0) - V_G^{\text{el}}(0)}{h} = \delta\nu_0\left(1 + \frac{\Delta\alpha_V}{2\Delta\alpha_S - \Delta\alpha_T}\sin(2\gamma)\right), \tag{10}$$

with $\delta\nu_0 = -(\Delta\alpha_S - \Delta\alpha_T/2)I_0/2hc\epsilon_0 = 1.48(5_{\text{stat}})$ MHz and $\Delta\alpha_V/(2\Delta\alpha_S - \Delta\alpha_T) = -4.46(1_{\text{stat}})$.

An important conclusion from our measurements is that there is a specific ellipticity parameter $\gamma^* = 6.5(2_{\text{stat}})^\circ$ [vertical dashed line in Fig. 5(c)] such that the differential light shift cancels for the two states $|g\rangle$ and $|e\rangle$. This is a so-called magic ellipticity and in this configuration the difference of energy between the two states is independent of the trap intensity. This condition proves particularly useful to realize robust probing or imaging of Dy atoms in a deep trap, as discussed earlier.

C. Polarizability measurement free from trap waist errors

The absolute value of the scalar polarizability that we extracted above is far from theoretical expectations (see the discussion below) and is accompanied by a large uncertainty due to the difficulty to calibrate the trap shape *in situ*. To get a more accurate value, we perform an *in situ* measurement of two observables, the trap frequency and the trap depth, which yields a measurement of the polarizability that is independent of the trap size, as was performed, for instance, using another species as a reference in [31]. This method is valid for any trap intensity profile whose radial dependence is defined by a single length scale: $I(r) = \frac{P}{2\pi l_r^2} f(r/l_r)$. For Gaussian beams or diffraction-limited beams (3) as is the case here, the following relationship holds:[3]

$$\left(\frac{U_0}{\omega_\perp}\right)^2 = \frac{\alpha m P}{4\pi c\varepsilon_0}. \tag{11}$$

[3]Equation (11) holds assuming $\zeta = -\frac{f(0)^2}{f''(0)} = 1$. This is true for Gaussian or diffraction-limited beams, but for higher-order ones such as Laguerre-Gauss beams, one then needs to multiply the right-hand side of (11) by ζ.

Here U_0 is the potential depth of a tweezer in the ground state, $\omega_\perp$ is the radial trapping frequency, and P is the beam power. One then only needs to measure P, $\omega_\perp$ and U_0 for the same trap to extract α. While the two former are straightforward, we use here a method based on single atoms in moving tweezers to measure U_0.

To do so, we rely on the fact that the single-atom tweezer's position is controllable in real time by the acousto-optic deflector that produces the traps. We perform a sequence where we place an atom in a tweezer, which we adiabatically accelerate to a given velocity v_g in the direction perpendicular to the chain. In a tweezer, the atom is at rest in the moving frame of the tweezer, but reaches the velocity v_g in the laboratory frame. We then abruptly stop the tweezer. The atom now has a kinetic energy $E_K = \frac{1}{2}mv_g^2$ in the trap frame. If E_K is smaller than the trap depth U_0, the atom will remain in the trap. However, if E_K is larger than U_0, the atom will be expelled from the trap. The exact trajectory followed by the traps is shown in Fig. 6(a). At time $t = 0$, the trap is slowly accelerated until it reaches the constant velocity v_g where it is then abruptly stopped. Typically, the distance covered by the trap in this time is $\Delta x = 43(1_{\text{sys}})$ μm and we change the velocity v_g reached at the end of the motion by scanning the acceleration time t_a between 1 and 5 ms. We can then look for the threshold in velocity v_g given to the atoms under which they remain in the trap [see Fig. 6(b)].

In practice, the threshold is broadened by the nonzero atomic temperature. The initial velocity v of the atom in the direction of motion follows the Boltzmann distribution

$$P(v) = \sqrt{\frac{m}{2\pi k_B T}} \exp\left(-\frac{1}{2}\frac{mv^2}{k_B T}\right).$$

After the trap has stopped, the atom then has the kinetic energy $E_K(v) = \frac{1}{2}m(v + v_g)^2$. The probability that the atom remains in the trap is then

$$P_S = \int \Theta(U_0 - E_K(v))P(v)\mathrm{d}v = \frac{1}{2}\left[\mathrm{erf}\left(\sqrt{\frac{U_0}{k_B T}} + \sqrt{\frac{U_g}{k_B T}}\right) + \mathrm{erf}\left(\sqrt{\frac{U_0}{k_B T}} - \sqrt{\frac{U_g}{k_B T}}\right)\right], \tag{12}$$

where $U_g = \frac{1}{2}mv_g^2$ is the kinetic energy imparted by the tweezer movement. Thus, under the assumption of adiabaticity, the result of this experiment only depends on the trap depth and atomic temperature, but does not depend on the exact trap shape.

In Fig. 6(b) we show the result of experiments performed in parallel on 50 tweezers whose powers have been equalized [9]. We ensure that the polarization is homogeneous across the traps by placing a Glan-Thompson polarizer directly after the AOD. Atoms are imaged once before the movement and once after. Averaging over the 50 tweezers and many realizations yields the recapture probability P_S for a given velocity v_g. The green solid line is a fit with Eq. (12), which yields a trap depth of $U_0 = k_B \times 119(7_{\text{sys}})(1_{\text{stat}})$ μK and a temperature $T = 5.5(4_{\text{stat}})$ μK for a tweezer power of $1.7(3_{\text{sys}})$ mW. We find that this temperature is in excellent agreement with

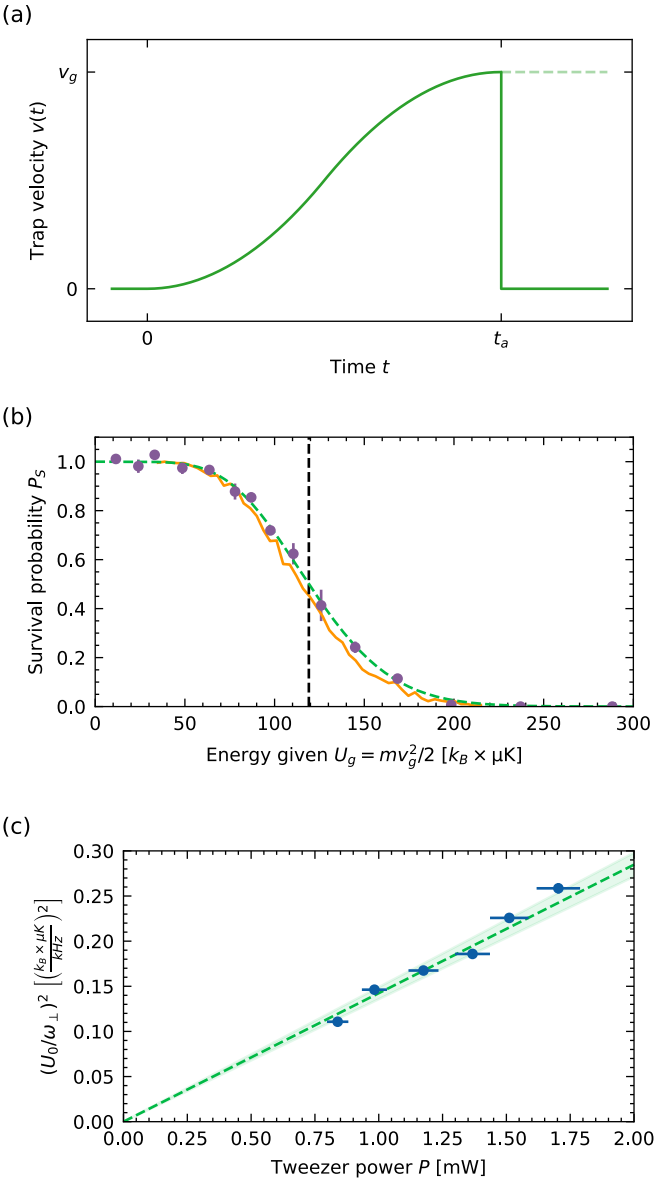

FIG. 6. (a) Trajectory followed by the trap to measure the trap depth. The trap is adiabatically accelerated to a velocity v_g and then abruptly brought to a stop. (b) Fraction of atoms that survive the abrupt stop of the traps initially moving at the velocity v_g. Purple points are experimental measurements. They are corrected to take into account losses during imaging. The green dashed line is a fit using Eq. (12). The orange solid line shows results of 3D simulations of atoms in a moving Gaussian trap. The dashed vertical line indicates the trap depth. (c) Evolution of $(U_0/\omega_\perp)^2$ for different tweezer powers. Blue dots are experimental points. The green dashed line is a linear fit to the data.

the usual release-recapture method [9]. We have verified that numerical simulations of the Newton equations of motion for atoms in a moving Gaussian trap reproduce very well the results [orange solid line in Fig. 6(b)]. In Fig. 6(c) we show the value of $(U_0/\omega_\perp)^2$ obtained for variable tweezer power, exhibiting a linear dependence. A linear fit gives the atomic polarizability of $\alpha = 204(40_{\text{sys}})(5_{\text{stat}})\alpha_0$. This measurement was realized on single atoms, in the magic imaging

TABLE I. Listed on the left-hand side are the experimentally measured polarizabilities for the ground state and the upper state of the intercombination line at 532 nm, in atomic units ($\alpha_0 = 1.649 \times 10^{-41}$ C^2 m^2 J^{-1}). Values in parentheses are the quadratic sums of systematic and statistical uncertainties. On the right-hand side are the theoretical values and their estimated uncertainties.

Experiment			Theory		
Polarizability	G	E	Polarizability	G	E
α_S	180(36)	130(40)	α_S	408(56)	73(30)
α_V	4(15)	260(80)	α_V	−57(93)	125(60)
α_T	−25(12)	−68(18)	α_T	−18(61)	−44(38)

configuration with a polarization ellipse perpendicular to the magnetic field and with ellipticity parameter $\gamma^* = 6.5$. In this configuration $\alpha = \alpha_S^G - \alpha_T^G/2 + \alpha_V^G/2\sin(2\gamma^*)$. Using the values of the atomic polarizability ratios from Sec. III A, we obtain a better estimate of the ground-state scalar polarizability $\alpha_S^G = 180(35_{\text{sys}})(10_{\text{stat}})\alpha_0$. This value is compatible with the one obtained in the previous section [$\alpha_S^G = 150(100_{\text{sys}})(30_{\text{stat}})\alpha_0$] in a different trap, ruling out a large systematic error not taken into account.

IV. COMPARISON WITH CALCULATIONS

We use the more accurate estimation of the absolute value of α_S^G obtained in Sec. III C in addition to the ratios measured in Secs. III A and III B to calculate all the polarizabilities in the ground state and excited state. They are summarized in Table I on the left-hand side and in Fig. 7. We discuss below how they compare with theoretical expectations.

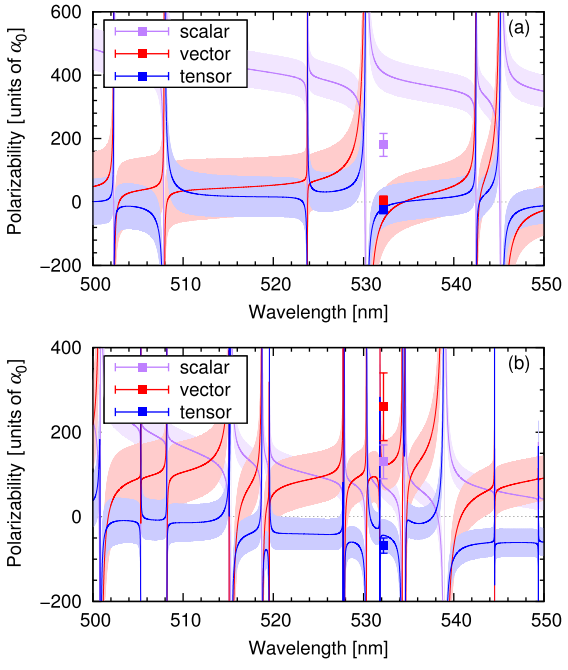

FIG. 7. Calculated scalar (purple), vector (red), and tensor (blue) polarizabilities, as well as their uncertainties, as a function of the trap wavelength, of (a) the level $|G\rangle$ and (b) the level $|E\rangle$. Experimental values at 532.208 nm are also shown with their error bars.

We report in Table I on the right-hand side and in Fig. 7 the theoretical expectations for the polarizabilities and their uncertainties obtained by using the methods presented in [29,36] and modified in such a way that when they are known, experimental level energies are included in a sum-over-states formulas. We consider that the uncertainty in polarizabilities comes from the uncertainty in theoretical line strengths, for which Ref. [36] gives an average value of 12.4%. Each term of the sum-over-state formulas brings to the uncertainty a contribution equal to its absolute value multiplied by 12.4%. As one can see, despite the rather large uncertainties, the experimental polarizabilities that we obtained do not all agree with theoretical expectations.

In particular, the disagreement is sizable for the scalar polarizability, with the experiment a factor 2 below expectations. The measured ground-state polarizability is close to that measured at 1064 nm [$\alpha_S = 184.4(2.4)\alpha_0$, in agreement with calculations at that wavelength performed with the same method] [31]. Since the wavelength of 532 nm is closer to the strong blue transitions of Dy, which are mainly contributing to the scalar polarizability α_S, one would expect α_S to be higher at this wavelength than at 1064 nm, as predicted in [36]. A lower value could be explained if there was a nearby transition from which the trap wavelength (precisely 532.208 nm) would be blue detuned. The closest candidate would be the level at 18 528.55 cm^{-1} (corresponding to a transition wavelength of 539.708 nm). However, its transition with the ground state has not been detected [37] and our calculations predict an Einstein coefficient $A_{ik} \approx 7 \times 10^4$ s^{-1}, much too weak to affect α_S at 532 nm. On the contrary, our trap wavelength is red detuned with respect to the level at 18 857.04 cm^{-1} (530.306 nm), which tends to increase the scalar polarizability. Moreover, our theoretical calculations including the configuration [Xe]4f^{9}5d^{2}6s do not predict any experimentally unknown level in this region of the Dy spectrum.

Regarding the other values, we note that the vector and tensor polarizabilities in the ground state and excited state do not perfectly agree but fall within the ranges of uncertainty. However, since these value are extracted from the knowledge of the ground scalar polarizability, the mismatch would be higher if it was wrong by a factor 2. Since the experimental methods used here are free of errors on the trapping laser intensity and consistent over several measurements, the origin of the theory-experiment disagreement remains yet unknown. The present work thus begs for future investigations to understand this large discrepancy.

V. CONCLUSION

We have presented an experimental apparatus where a MOT of Dy in a glass cell is continuously loaded from a 2D MOT. This MOT allows one to load optical tweezers at 532 nm. We reported here measurements of all components of the polarizability on the intercombination transition. We found a remarkably low scalar polarizability in the ground state, which calls for future investigations. Our setup allowed us to image single atoms in magic tweezers with greater than 99% fidelity and about 2.5% loss probability in a single

image, allowing for many future studies using the tweezers toolbox.

To improve imaging fidelity when using the intercombination line, we expect that it would be beneficial to use optical tweezers with a longer wavelength, which would suppress excitation of atoms to high-lying metastable states. One could use, for instance, the magic condition found in [29]. Finally, in this work we used exclusively the bosonic ^{162}Dy isotope, which has no hyperfine structure. However, we expect that fermionic isotopes with their hyperfine structure might present different and possibly advantageous mechanisms for imaging and deterministic loading of the tweezers, as was observed, for example, on ytterbium [24].

ACKNOWLEDGMENTS

We thank Florence Nogrette for experimental help and discussions. We note that another setup based on a similar 421-nm 2D MOT loading a 626-nm 3D MOT of Dy atoms has been developed by the group of L. Chomaz [10]. We have widely benefited from exchanges between our groups. This work received funding from the Agence Nationale de la Recherche (JCJC grant DEAR, Grant No. ANR-22-PETQ-0004 France 2030, and project QuBitAF), the European Union (ERC StG CORSAIR Grant No. 101039361 and ERC AdG ATARAXIA Grant No. 101018511), and the Horizon Europe program HORIZON-CL4-2022-QUANTUM-02-SGA [Project No. 101113690 (PASQuanS2.1)].

[1] L. Chomaz, I. Ferrier-Barbut, F. Ferlaino, B. Laburthe-Tolra, B. L. Lev, and T. Pfau, Dipolar physics: A review of experiments with magnetic quantum gases, Rep. Prog. Phys. **86**, 026401 (2023).

[2] D. Barredo, S. de Léséleuc, V. Lienhard, T. Lahaye, and A. Browaeys, An atom-by-atom assembler of defect-free arbitrary two-dimensional atomic arrays, Science **354**, 1021 (2016).

[3] M. Endres, H. Bernien, A. Keesling, H. Levine, E. R. Anschuetz, A. Krajenbrink, C. Senko, V. Vuletic, M. Greiner, and M. D. Lukin, Atom-by-atom assembly of defect-free one-dimensional cold atom arrays, Science **354**, 1024 (2016).

[4] H. Kim, W. Lee, H.-g. Lee, H. Jo, Y. Song, and J. Ahn, *In situ* single-atom array synthesis using dynamic holographic optical tweezers, Nat. Commun. **7**, 13317 (2016).

[5] W. S. Bakr, J. I. Gillen, A. Peng, S. Fölling, and M. Greiner, A quantum gas microscope for detecting single atoms in a Hubbard-regime optical lattice, Nature (London) **462**, 74 (2009).

[6] J. F. Sherson, C. Weitenberg, M. Endres, M. Cheneau, I. Bloch, and S. Kuhr, Single-atom-resolved fluorescence imaging of an atomic Mott insulator, Nature (London) **467**, 68 (2010).

[7] L. Su, A. Douglas, M. Szurek, R. Groth, S. F. Ozturk, A. Krahn, A. H. Hébert, G. A. Phelps, S. Ebadi, S. Dickerson, F. Ferlaino, O. Marković, and M. Greiner, Dipolar quantum solids emerging in a Hubbard quantum simulator, Nature (London) **622**, 724 (2023).

[8] G. Anich, R. Grimm, and E. Kirilov, Comprehensive characterization of a state-of-the-art apparatus for cold electromagnetic dysprosium dipoles, arXiv:2304.12844.

[9] D. Bloch, B. Hofer, S. R. Cohen, A. Browaeys, and I. Ferrier-Barbut, Trapping and imaging single dysprosium atoms in optical tweezer arrays, Phys. Rev. Lett. **131**, 203401 (2023).

[10] S. Jin, J. Gao, K. Chandrashekara, C. Gölzhäuser, J. Schöner, and L. Chomaz, A 2D MOT of dysprosium atoms as a compact source for efficient loading of a narrow-line 3D MOT, Phys. Rev. A **108**, 023719 (2023).

[11] M. A. Norcia, A. W. Young, and A. M. Kaufman, Microscopic control and detection of ultracold strontium in optical-tweezer arrays, Phys. Rev. X **8**, 041054 (2018).

[12] A. Cooper, J. P. Covey, I. S. Madjarov, S. G. Porsev, M. S. Safronova, and M. Endres, Alkaline-earth atoms in optical tweezers, Phys. Rev. X **8**, 041055 (2018).

[13] S. Saskin, J. T. Wilson, B. Grinkemeyer, and J. D. Thompson, Narrow-line cooling and imaging of ytterbium atoms in an optical tweezer array, Phys. Rev. Lett. **122**, 143002 (2019).

[14] I. Nosske, L. Couturier, F. Hu, C. Tan, C. Qiao, J. Blume, Y. H. Jiang, P. Chen, and M. Weidemüller, Two-dimensional magneto-optical trap as a source for cold strontium atoms, Phys. Rev. A **96**, 053415 (2017).

[15] M. Barbiero, M. G. Tarallo, D. Calonico, F. Levi, G. Lamporesi, and G. Ferrari, Sideband-enhanced cold atomic source for optical clocks, Phys. Rev. Appl. **13**, 014013 (2020).

[16] S. Eckel, D. S. Barker, E. B. Norrgard, and J. Scherschligt, PyLCP: A Python package for computing laser cooling physics, Comput. Phys. Commun. **270**, 108166 (2022).

[17] E. Wodey, R. J. Rengelink, C. Meiners, E. M. Rasel, and D. Schlippert, A robust, high-flux source of laser-cooled ytterbium atoms, J. Phys. B **54**, 035301 (2021).

[18] T. Maier, H. Kadau, M. Schmitt, A. Griesmaier, and T. Pfau, Narrow-line magneto-optical trap for dysprosium atoms, Opt. Lett. **39**, 3138 (2014).

[19] D. Dreon, L. A. Sidorenkov, C. Bouazza, W. Maineult, J. Dalibard, and S. Nascimbene, Optical cooling and trapping of highly magnetic atoms: The benefits of a spontaneous spin polarization, J. Phys. B **50**, 065005 (2017).

[20] J. Lee, J. H. Lee, J. Noh, and J. Mun, Core-shell magneto-optical trap for alkaline-earth-metal-like atoms, Phys. Rev. A **91**, 053405 (2015).

[21] S. H. Youn, M. Lu, U. Ray, and B. L. Lev, Dysprosium magneto-optical traps, Phys. Rev. A **82**, 043425 (2010).

[22] J. Höschele, S. Buob, A. Rubio-Abadal, V. Makhalov, and L. Tarruell, Atom-number enhancement by shielding atoms from losses in strontium magneto-optical traps, Phys. Rev. Appl. **19**, 064011 (2023).

[23] S. Ma, A. P. Burgers, G. Liu, J. Wilson, B. Zhang, and J. D. Thompson, Universal gate operations on nuclear spin qubits in an optical tweezer array of ^{171}Yb atoms, Phys. Rev. X **12**, 021028 (2022).

[24] A. Jenkins, J. W. Lis, A. Senoo, W. F. McGrew, and A. M. Kaufman, Ytterbium nuclear-spin qubits in an optical tweezer array, Phys. Rev. X **12**, 021027 (2022).

[25] S. Kotochigova and A. Petrov, Anisotropy in the interaction of ultracold dysprosium, Phys. Chem. Chem. Phys. **13**, 19165 (2011).

[26] M. Lepers, J.-F. Wyart, and O. Dulieu, Anisotropic optical trapping of ultracold erbium atoms, Phys. Rev. A **89**, 022505 (2014).

[27] W. Kao, Y. Tang, N. Q. Burdick, and B. L. Lev, Anisotropic dependence of tune-out wavelength near Dy 741-nm transition, Opt. Express **25**, 3411 (2017).

[28] J. H. Becher, S. Baier, K. Aikawa, M. Lepers, J.-F. Wyart, O. Dulieu, and F. Ferlaino, Anisotropic polarizability of erbium atoms, Phys. Rev. A **97**, 012509 (2018).

[29] T. Chalopin, V. Makhalov, C. Bouazza, A. Evrard, A. Barker, M. Lepers, J.-F. Wyart, O. Dulieu, J. Dalibard, R. Lopes, and S. Nascimbene, Anisotropic light shift and magic polarization of the intercombination line of dysprosium atoms in a far-detuned dipole trap, Phys. Rev. A **98**, 040502(R) (2018).

[30] M. Kreyer, J. H. Han, C. Ravensbergen, V. Corre, E. Soave, E. Kirilov, and R. Grimm, Measurement of the dynamic polarizability of Dy atoms near the 626-nm intercombination line, Phys. Rev. A **104**, 033106 (2021).

[31] C. Ravensbergen, V. Corre, E. Soave, M. Kreyer, S. Tzanova, E. Kirilov, and R. Grimm, Accurate determination of the dynamical polarizability of dysprosium, Phys. Rev. Lett. **120**, 223001 (2018).

[32] T. Maier, Interactions in a quantum gas of dysprosium atoms, Ph.D. thesis, University of Stuttgart, 2015.

[33] M. Schmitt, A self-bound dilute quantum liquid of dysprosium atoms, Ph.D. thesis, University of Stuttgart, 2017.

[34] F. Le Kien, P. Schneeweiss, and A. Rauschenbeutel, Dynamical polarizability of atoms in arbitrary light fields: General theory and application to cesium, Eur. Phys. J. D **67**, 92 (2013).

[35] C. Cohen-Tannoudji and J. Dupont-Roc, Experimental study of Zeeman light shifts in weak magnetic fields, Phys. Rev. A **5**, 968 (1972).

[36] H. Li, J.-F. Wyart, O. Dulieu, S. Nascimbène, and M. Lepers, Optical trapping of ultracold dysprosium atoms: Transition probabilities, dynamic dipole polarizabilities and van der Waals C_6 coefficients, J. Phys. B **50**, 014005 (2017).

[37] M. Wickliffe, J. E. Lawler, and G. Nave, Atomic transition probabilities for Dy I and Dy II, J. Quant. Spectrosc. Radiat. Transfer **66**, 363 (2000).